

# TOWARD A RAYLEIGH WAVE ATTENUATION MODEL FOR ASIA AND SURROUNDING REGIONS

Anatoli L. Levshin<sup>1</sup>, Mikhail P. Barmin<sup>1</sup>, Xiaoning Yang<sup>2</sup>, Michael H. Ritzwoller<sup>1</sup>

University of Colorado at Boulder<sup>1</sup>, Los Alamos National Laboratory<sup>2</sup>

Sponsored by National Nuclear Security Administration

Contract Nos. DE-FC52-05NA26608<sup>1</sup>, and DE-AC52-06NA25396<sup>2</sup>

## **ABSTRACT**

We report on the progress toward the development of attenuation models for short-period (12-22 sec) Rayleigh waves in Asia and surrounding regions. This model is defined by maps of attenuation coefficients across the region of study in the specified period band. The model is designed to calibrate the regional surface-wave magnitude scale and to extend the teleseismic ‘surface-wave magnitude – body-wave magnitude’ ( $M_s$ - $m_b$ ) discriminant to regional distances.

In order to obtain accurate attenuation estimates, we must first measure surface-wave amplitudes reliably. Taking advantage of certain characteristics of Rayleigh waves, such as the dispersion and the elliptical particle motion, we employed a suite of techniques in making accurate fundamental-mode Rayleigh-wave amplitude measurements. We first analyze the dispersion of the surface wavetrain using a spectrogram. Based on the characteristics of the data dispersion, we design a phase-matched filter by using either a manually picked dispersion curve, or a model-predicted dispersion curve, or the dispersion of the data, and apply the filter to the seismogram. Intelligent filtering of the seismogram and windowing of the resulting cross-correlation based on the spectrogram analysis and the comparison between the spectrum of phase-match filtered data and raw-data and source spectra effectively reduces amplitude contaminations from surface-wave higher modes, multipathing, body-wave energy and other noise sources, and results in reliable amplitude measurements in many cases. We implemented these measuring techniques in a graphic-user-interface tool called Surface Wave Amplitude Measurement Tool (SWAMTOOL). Using the tool, we collected and processed waveform data for 200 earthquakes occurring throughout 2003-2006 inside and around Eurasia. The records from 135 broadband permanent and temporary stations were used.

After obtaining surface-wave amplitude measurements, we analyzed the attenuation behavior of the amplitudes using source- and receiver-specific terms calculated from the three-dimensional (3D) velocity model CUB2 of the region. Based on the results, we removed amplitudes that yielded negative average attenuation coefficients, and included an additional parameter in the inversion to account for the possible bias in Harvard Centroid Moment Tensor (CMT) (Dziewonski *et al.*, 1981) scalar moments. We used the tomographic inversion to obtain surface-wave attenuation-coefficient maps from 12 to 22 seconds for Asia and surrounding regions. The inverted attenuation maps are consistent with geological features of Asia. We observe low attenuations in stable regions such as eastern Europe, the Siberian platforms, the Indian Shield, the Arabian platform, the Yangtze Craton, and others. High attenuation is observed in tectonically active regions such as the Himalayas, the Tian Shan, Pamir and Zagros mountains. Finally, we conducted the calibration of a new  $M_s$  formula (Russell, 2006) for the same region using 3D group-velocity models.

## **OBJECTIVES**

The objectives of the study are 1) to develop short-period (12 – 22s), two-dimensional (2D) Rayleigh-wave attenuation maps for Asia and surrounding regions along with associated uncertainty statistics through a tomographic approach, and 2) to calibrate Russell's (2006)  $M_s$  formula with these maps for the same region.

Knowledge of the seismic-energy loss during the propagation of surface waves from the source to receivers is essential for the accurate estimation of the surface-wave magnitude  $M_s$  and the seismic moment of the source. This is especially important for nuclear-explosion monitoring, in which  $M_s$  is used in the most robust seismic discriminant, the  $M_s$ - $m_b$  discriminant. In order to apply this discriminant to regional-distance monitoring, a modified  $M_s$  formula using shorter-period (< 20 s) surface-wave amplitudes is required (e.g., Marshall and Basham, 1970; Russell, 2006). At regional distances, seismic-wave propagation is strongly influenced by the lateral heterogeneity of the crust and upper-mantle material properties. Short-period, 2D surface-wave attenuation maps developed from observed amplitude data used to correct for the propagation effects in calculating  $M_s$  hold the potential to reduce station-magnitude scatter and network-magnitude bias. In this paper, we describe the surface-wave amplitude collection and measurement, the development of the attenuation models, and the Russell (2006)  $M_s$  calibration results.

## **RESEARCH ACCOMPLISHED**

### **Surface-Wave Data Collection and Amplitude Measurement**

Surface-wave amplitudes could be contaminated by a variety of sources such as multipathing, focusing and defocusing, body wave, higher-mode surface wave, and other noise sources. In order to obtain accurate attenuation estimates, we must measure surface-wave amplitudes reliably by reducing the contamination as much as possible. Taking advantage of certain characteristics of Rayleigh waves, such as the dispersion and the elliptical particle motion, we employed a suite of techniques in making accurate fundamental-mode Rayleigh-wave amplitude measurements. We first analyze the dispersion of the surface wavetrain using a spectrogram. Based on the characteristics of the data dispersion, we design a phase-matched filter by using either a manually picked dispersion curve, or a model-predicted dispersion curve, or the dispersion of the data, and apply the filter to the seismogram. Intelligent filtering of the seismogram and windowing of the resulting cross-correlation based on the spectrogram analysis and the comparison between spectrum of phase-match filtered data and raw-data and source spectra effectively reduces amplitude contaminations from surface-wave higher modes, multipathing, body-wave energy and other noise sources, and results in reliable amplitude measurements in many cases.

We implemented these measuring techniques in a graphic-user-interface tool called Surface Wave Amplitude Measurement Tool (SWAMTOOL). Figure 1 is a computer-screen snapshot of SWAMTOOL. The tool consists of four panels showing the seismograms (upper right), a map (lower right), the data spectrogram (upper left), and the spectra of the source, the data and the noise (lower left). Surface-wave segment is first isolated with the guidance of nominal group-velocity marks, shown as red vertical dashed lines in the top figure of the seismogram panel, and the dispersion characteristics predicted by 2D group-velocity models (Ritzwoller and Levshin, 1998; Levshin and Ritzwoller, 2003; Stevens *et al.*, 2001; Levshin *et al.*, 2003), depicted as open red circles in the spectrogram panel. A phase-matched filter is then constructed with a dispersion curve (red line in the spectrogram panel) determined by analyzing the surface-wave spectrogram and the dispersion predicted by the group-velocity models. Depending on the characteristics of the data dispersion, we use either a manually determined dispersion curve, or the dispersion curve of the data, or the dispersion curve predicted by the group-velocity model to construct the phase-matched filter. Surface-wave spectral amplitudes (red line in the spectrum panel) are measured after the seismogram is processed with phase-match filtering and windowing. We use theoretic source spectrum (green line in the spectrum panel) as a reference for windowing the cross-correlation resulting from the phase-match filtering (middle figure in the seismogram panel), taking into account of the source-depth uncertainty (black lines bracketing the green region in the spectrum panel.) We also calculate the backazimuth of the incoming Rayleigh wave and compare it with the great-circle backazimuth. The result is displayed at the lower left of the map panel. Other information displayed in the tool includes the average  $Q$  between the source and the station at 10, 15 and 20 sec (in the spectrum panel), noise spectrum (blue line in the spectrum panel), and source and path information in the map panel. Finally, the usable frequency band of the measured spectrum is determined by the yellow region in the spectrum panel. Figure 1 shows

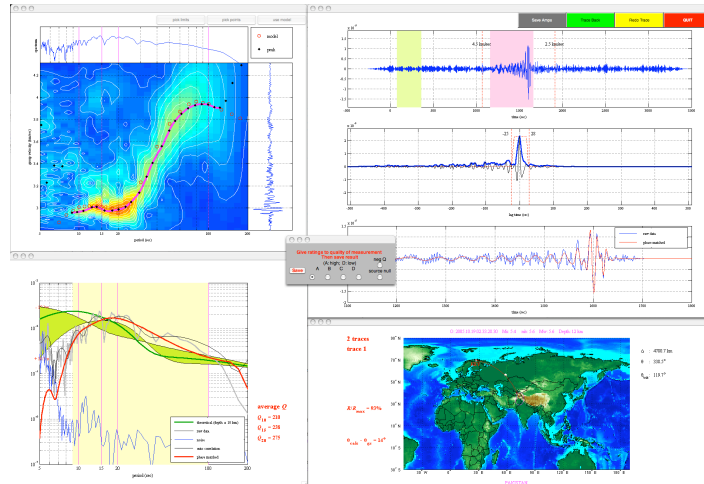


**Figure 1. A computer-screen snapshot of SWAMTOOL. It shows an example where the medium between the source and the receiver is relatively simple with weak lateral heterogeneities. The seismogram possesses well-behaved dispersion characteristics, which is also predicted by the group-velocity model. The spectrum of phase-match filtered data does not differ significantly from the spectrum of the raw data.**

an example where the medium between the source and the receiver is relatively homogeneous. Figure 2 gives an example illustrating how multipathing is treated. An example showing the reduction of noise from body waves and other sources using the tool is given in Figure 3.

We collected and processed waveform data for 200 earthquakes occurring throughout 2003–2006 in and around Eurasia. The magnitudes of these events range from 5 to 6. Source depths are less than 70 km. Data from 135 broadband permanent and temporary stations were used. Using SWAMTOOL, we made both two-station amplitude

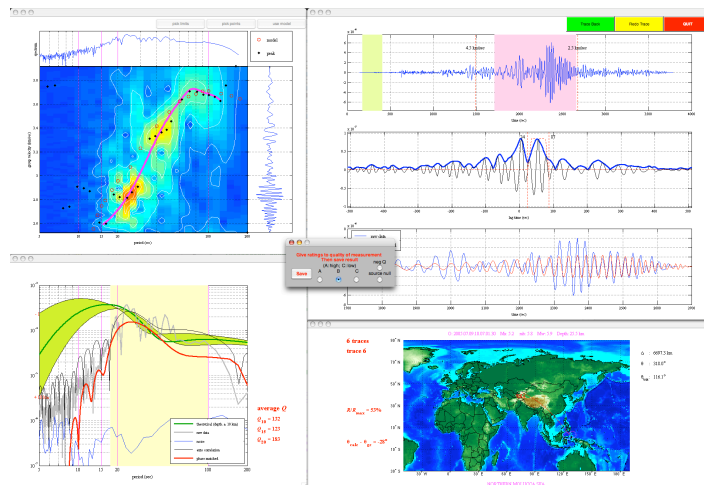


**Figure 2. This example illustrates how the effects of multipathing and focusing are mitigated by using SWAMTOOL. In this example, the surface wave from the source traverses the Tarim Basin, resulting in surface-wave packets traveling along different paths and arriving at the receiver at slightly different times. The cross-correlation from phase-match filtering shows two peaks corresponding to the two surface-wave packets, although they are difficult to distinguish in the spectrogram due to the similarity of their travel times. Windowing of the cross-correlation removes one of the surface-wave packets and reduces the effects of multipathing and focusing.**

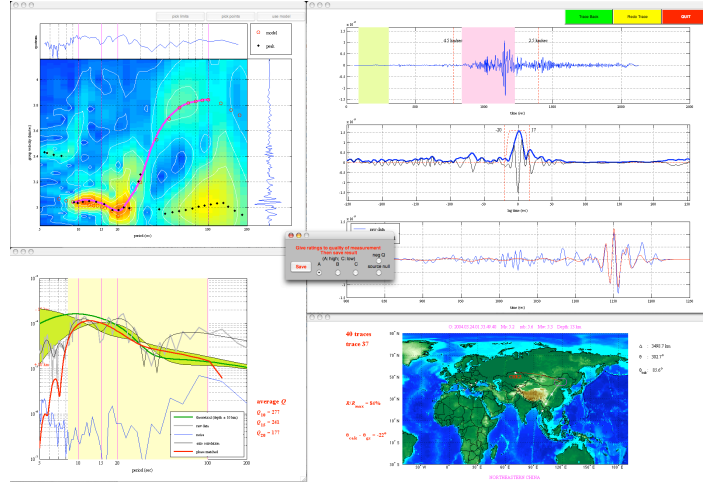


**Figure 3.** This figure is an example in which surface-wave signal is contaminated by body waves and signals from other sources. The spectrogram shows strong signals from other sources, in addition to the fundamental-mode surface wave. Because signals from sources other than the surface wave have different dispersion characteristics, the application of phase-matched filter and windowing can effectively remove these signals partly because they appear as signal packets in the cross-correlation at different lag-times from that of the surface wave.

ratio and single-station spectral-amplitude measurements, but only single-station amplitudes are used in later tomographic inversions. Figure 4 shows the path coverage of single-station amplitude measurements at different periods.

### Amplitude Selection Based on Average Attenuation Analysis

Before using measured amplitudes in the tomographic inversion, we estimated the average attenuation between sources and receivers from the measurements. Measurements that yielded negative attenuation coefficients were rejected. We used the theoretical surface-wave amplitude formula for a heterogeneous Earth (Woodhouse, 1974; Levshin, 1985; Levshin *et al.*, 1989) to estimate the average attenuation. For a laterally heterogeneous medium, the spectral amplitude of a surface wave can be expressed in an asymptotic form as:

$$A(\omega) = S(\omega, h, \varphi)P(\omega)B(\omega), \quad (1)$$

where  $\omega$  is circular frequency;  $h$  is source depth and  $\varphi$  is station azimuth.  $S$ ,  $P$  and  $B$  are source, path and station terms respectively.  $S$  and  $B$  depend on the medium structures and properties at the source and receiver locations, which are generally different in a heterogeneous Earth. The path-dependent term  $P$  has the form

$$P = \frac{\exp\left(-\omega \int_L \frac{dl}{2U(\omega, l)Q_R(\omega, l)}\right)}{\sqrt{k(\omega)r_0 \sin \Delta}} = \frac{\exp\left(-\int_L \gamma_R(\omega, l)dl\right)}{\sqrt{k(\omega)r_0 \sin \Delta}}, \quad (2)$$

where  $\Delta$  is the epicentral distance;  $r_0$  is Earth's radius;  $U$  is the group velocity of the surface wave;  $k$  is the wavenumber;  $Q_R$  is the quality factor and  $\gamma_R$  is the attenuation coefficient. The integral is taken along the great-circle path between the source and the receiver. It represents the average attenuation of the path.

To obtain the average attenuation from measured amplitudes, we calculated theoretical source and receiver terms  $S$  and  $B$  using the 3D velocity model CUB2 (Shapiro and Ritzwoller, 2002) and CMT solutions. We then removed the source and receiver terms calculated for the specific source and receiver locations from measured amplitudes. Source- and receiver-corrected amplitudes were used to estimate the average attenuation.

#### EPICENTER-STATION PATHS

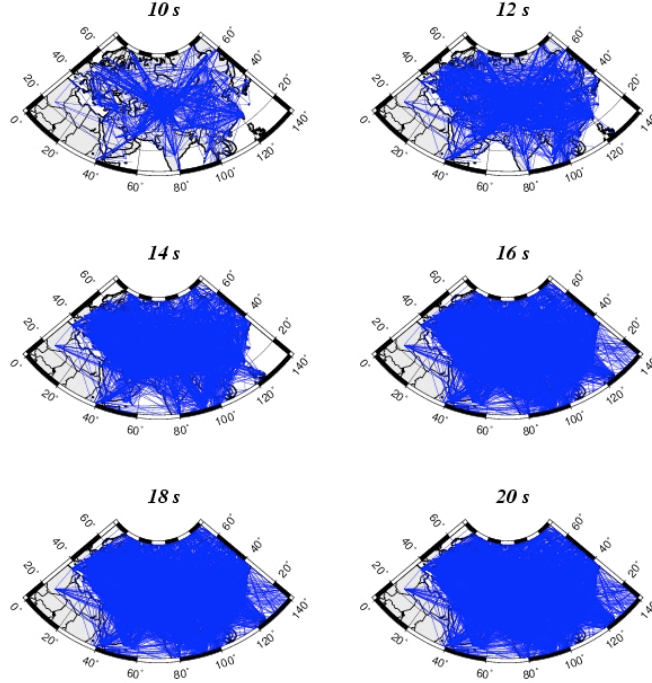


**Figure 4. Path coverage of single-station amplitude measurements at different periods.**

Figure 5 plots the logarithm of corrected amplitudes, indicative of the average attenuation, as a function of epicentral distance at 12, 16 and 20 seconds. The offset from zero of the least-squares-fitted line at zero distance indicates that there is a possible bias in CMT source parameters, consistent with the observation of Yang *et al.*, (2004). In addition, some of the estimated attenuation coefficients are negative, which is not physical. There are several possible explanations for obtaining negative attenuation coefficients. They include un-modeled site response, remaining contamination in the measured amplitudes, errors in the source parameter and inadequate description of the wave propagation by the ray theory (Eq. 2). We then removed the amplitudes that resulted in negative average attenuation coefficients from the subsequent tomographic inversion.

#### Attenuation-Coefficient Tomographic Inversion

We used the selected source- and receiver-corrected amplitudes in the attenuation-coefficient tomographic inversion to obtain attenuation-coefficient models for Asia and surrounding regions at periods between 12 and 22 seconds. We used a modified version of the inversion algorithm described by Barmin *et al.* (2001). The algorithm inverts for the attenuation-coefficient models by minimizing the functional

$$F(T) = \frac{1}{N} \sum_{ij} (d_{ij})^2 \quad (3)$$

at period  $T$ , where  $N$  is the total number of paths and  $d_{ij}$  is the amplitude residual between source  $i$  and station  $j$ :

$$d_{ij} = q_{ij}^{obs} - q_{ij}^0 = \int_{ij} m(\mathbf{r}) dl + \ln(\delta M_i). \quad (4)$$

$q_{ij}^{obs}$  is the value of the integral in Eq. (2) from measured amplitude.  $q_{ij}^0$  is the value of the integral from the attenuation model that we invert for.  $m(\mathbf{r})$  is the model perturbation from a reference model  $m_0(\mathbf{r})$ . The additional unknown parameter  $\delta M_i$  is included to account for the possible CMT moment bias.

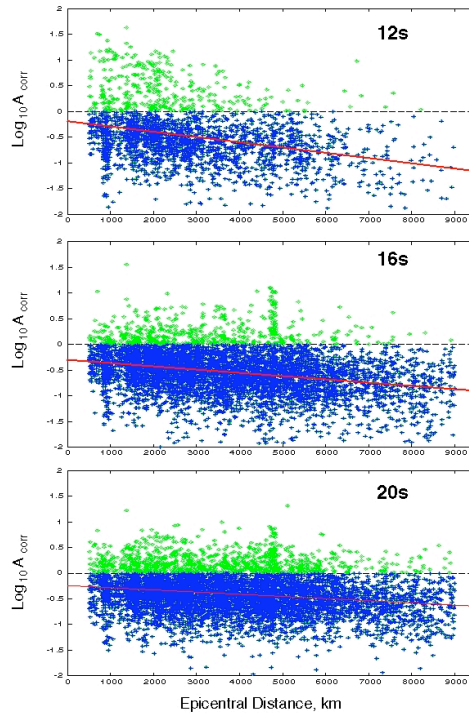


**Figure 5. Source- and receiver-corrected single-station spectral amplitudes plotted against epicentral distance. The red line is the least squares fit of the data. Green dots are data rejected from the tomographic inversion.**

We minimized  $F(T)$  using least squares and several damping parameters described in Barmin *et al.* (2001) with an additional damping parameter for  $\delta M_i$ . Eqs. (3) and (4) were used in the inversion of 18-sec amplitudes to obtain  $\delta M_i$ . The resulting  $M_{0i} = M_0 + \delta M_i$ , where  $M_0$  is the CMT scalar moment, was then used to correct the amplitudes for the source term at other periods, and  $\delta M_i$  was removed from the inversions. Numerous experiments with different values of damping parameters yielded the optimal inversion results. We also experimented with inversions in which we included  $\delta M_i$  for all the periods (“free” scalar-moment inversion.) The results are similar. The resulting tomographic models of attenuation coefficients  $\gamma_R$  for Asia and surrounding regions are shown in Figures 6. The attenuation models are consistent with geological features of Asia. We observe low attenuations in stable regions such as eastern Europe, the Siberian platforms, the Indian Shield, the Arabian platform, the Yangtze Craton, and others. High attenuation is observed in tectonically active regions such as the Himalayas, the Tian Shan, Pamir and Zagros mountains.

We estimated variance reductions achieved with our tomographic models by comparing their residual statistics with those of homogeneous models. For periods between 12 and 22 seconds, variance reduction is between 30% and 40% (Figure 7). Including a moment correction term  $\delta M_i$  in the inversion did further reduce the variance.

### **Calibration of Russell’s (2006) $M_s$ Formula for Asia**

Russell (2006) describes a new formulation of surface-wave magnitude using time-domain, Butterworth band-pass filtered amplitude. The new  $M_s$  is applicable for amplitudes measured at arbitrary periods and is not affected by the dispersion characteristics, including Airy-phase anomalies, of the surface waves because of the band-pass filtering. The ability of the Russell (2006)  $M_s$  to use amplitudes at variable periods is important in calculating regional surface-wave magnitude because at regional distances in continental regions, surface waves usually peak at periods

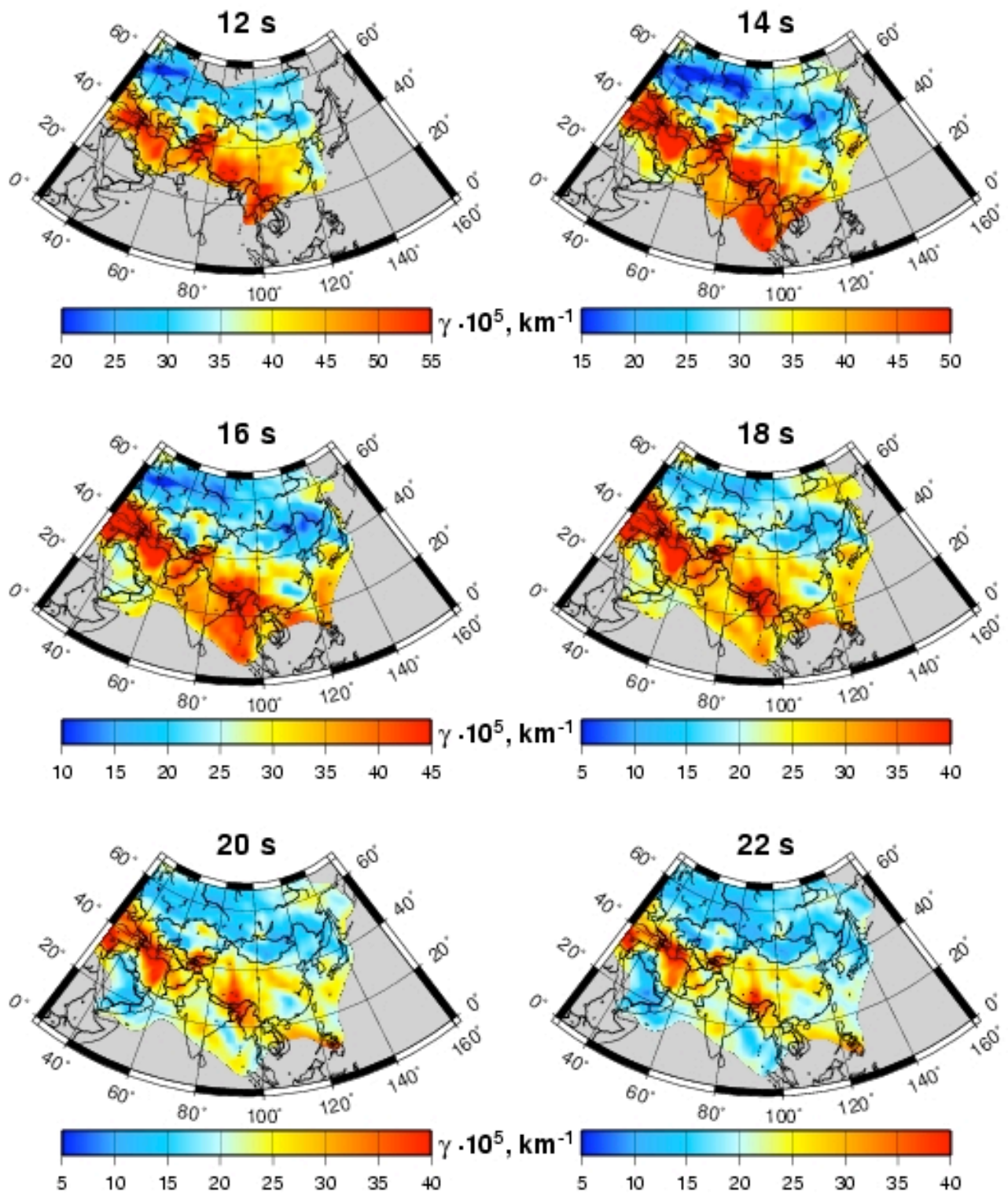
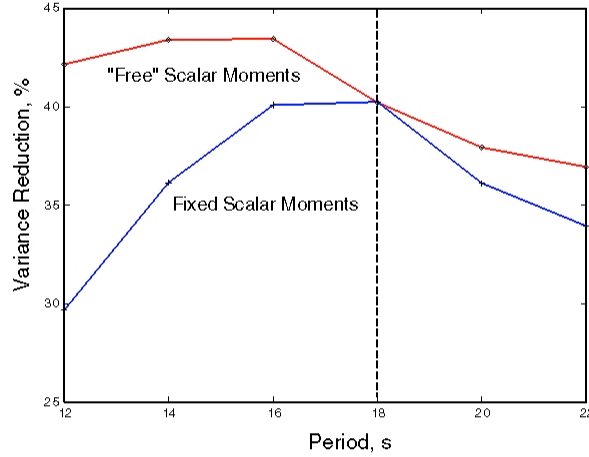


Figure 6. Tomographic models of attenuation coefficients across Asia and surrounding regions. Grey color corresponds to areas where the path density is less than 20 paths across an equatorial cell of  $2^\circ \times 2^\circ$ .



**Figure 7. Variance reduction of tomographic attenuation-coefficient models compared with homogeneous models. In “fixed-scalar-moment” inversions,  $\delta M_i$  obtained from the inversion of 18-sec amplitudes was used to correct the amplitudes for the source terms at other periods. In “free-scalar-moment” inversions,  $\delta M_i$  was included in inversions of amplitudes at all periods.**

that are shorter than 20 seconds, at which traditional surface-wave magnitudes are defined. The Russell (2006)  $M_s$  is defined as:

$$M_{S(b)} = \log_{10}(a_b) + \frac{1}{2} \log_{10}(\sin \Delta) + B_{att} \Delta - 0.66 \log_{10}\left(\frac{20}{T}\right) - \log_{10}(f_c) + C_b \quad (5)$$

and

$$f_c \leq \frac{G_{\min}}{T \sqrt{\Delta}},$$

where  $a_b$  is the time-domain, Butterworth band-pass filtered amplitude;  $\Delta$  is epicentral distance in degrees;  $B_{att}$  is related to the attenuation of the surface wave;  $T$  is the period of the amplitude and  $f_c$  is the half width of the Butterworth-filter pass band.  $G_{\min}$  is the minimum value of  $G$  where

$$G = \frac{U}{\pi b_n \sqrt{\left| \frac{dU}{dT} \right|} \kappa}. \quad (6)$$

$U$  and  $dU/dT$  are the surface-wave group velocity and its derivative with respect to period for the region of interest.  $b_n$  is related to the order of the Butterworth filter.  $\kappa$  is the degree-to-km converting factor. For typical continental regions, Russell (2006) found that  $G_{\min} = 0.6$  is adequate.  $C_b$  in Eq. (5) also depends on  $G$ .

To normalize the new  $M_s$  with traditional formulae such as Rezapour and Pearce’s (1998)  $M_s$ , Russell (2006) equated Eq. (5) with traditional formulae at  $\Delta = 50^\circ$  and derived formulae for  $B_{att}$  and  $C_b$ :

$$B_{att} = 0.0031 \left(\frac{20}{T}\right)^{1.8} \quad \text{and} \quad C_b = C + \log_{10}\left(\frac{G_0}{400}\right). \quad (7)$$

In the above formulae,  $C$  is the constant in traditional  $M_s$  formulae. Adopting the formulation of von Seggern (1977), Russell (2006) obtained a  $C$  value of 2.2 for  $a_b$  in nanometers.  $G_0$  is  $G$  at 20 seconds. Using nominal values of  $U$  and  $dU/dT$  at 20 seconds for continental regions, Russell (2006) derived a  $C_b$  value of -0.42 for a 6<sup>th</sup>-order Butterworth filter (Bonner, personal communication).

Bonner *et al.* (2006) developed a new amplitude measuring technique to be used along with the Russell (2006)  $M_s$  formula. They first band-pass filter the seismogram between 8 and 25 seconds using a bank of Butterworth filters.

From among the filtered data, they then find the time-domain amplitude that maximizes the ratio  $a_b/f_c$ , thus giving the maximum  $M_s$  (Eq. 5). The technique yields station magnitudes with significantly reduced scatter (Bonner *et al.*, 2006).

To calibrate Russell (2006)  $M_s$  for Asia, we collected seismograms from 100 events that occurred from 2002 to 2003 in Asia. We used Bonner *et al.*'s (2006) technique to measure the surface-wave amplitudes. We then calculated Russell (2006)  $M_s$  with Eq. (5) using the nominal parameter values derived by Russell (2006). We also calculated Prague  $M_s$  (Vaněk *et al.*, 1962) and Rezapour and Pearce (1998)  $M_s$  using amplitudes with periods in the band from 18 to 22 seconds. The Rezapour and Pearce (1998)  $M_s$  is currently used at the International Data Centre (IDC) as the standard  $M_s$  measurement. The Russell (2006)  $M_s$  that we calculated using the nominal parameter values with this dataset is, on the average, about 0.12 magnitude unit (mu) larger than the Rezapour and Pearce (1998)  $M_s$  calculated with the same dataset. The mean station-magnitude variance of the Russell (2006)  $M_s$  is, on the other hand, 17% smaller than that of the Rezapour and Pearce (1998)  $M_s$  and 58% smaller than that of the Prague  $M_s$ , consistent with the conclusion of Bonner *et al.* (2006).

To derive the parameter  $C_b$  in Eq. (7) that is specific for Asia, we utilized the surface-wave group-velocity models developed by Levshin *et al.* (2003). We first converted velocity to slowness. We then took the arithmetic mean of the slowness for all model nodes as the average slowness for the whole region. The average group velocity and its derivative (Eq. 6) were then derived from the average slowness. From the average group velocity and its derivative at 20 seconds, we obtained a  $G_0$  value of 0.72. Using this  $G_0$  in Eq (7), we obtained an Asia-specific  $C_b$  of -0.54. This value is 0.12 mu smaller than the nominal value of -0.42 derived by Russell (2006). If we use this value in Eq (5) to calculate the Russell (2006)  $M_s$  with the dataset that we collected, the average  $M_s$  will be the same as the average of Rezapour and Pearce (1998)  $M_s$  from the same dataset.

Another parameter in the Russell (2006)  $M_s$  formula is  $G_{\min}$  in Eq. (5). Instead of using the nominal value of 0.6 as Russell (2006) suggested, we derived  $G_{\min}$  based on the  $G$  values calculated from the group-velocity model. We then use the Asia-specific  $G_{\min}$ , with 0.6 as the upper bound, to define the bandwidth  $f_c$  of the Butterworth filters used in filtering the data and in the  $M_s$  calculation. The Russell (2006)  $M_s$  calculated using this procedure has an even smaller station-magnitude variance. The mean station-magnitude variance of the Russell (2006)  $M_s$  is now 22% smaller than that of the Rezapour and Pearce (1998)  $M_s$ . The Russell (2006)  $M_s$  itself is increased by 0.04 mu on average.

## **CONCLUSIONS AND RECOMMENDATIONS**

We developed a surface-wave amplitude-measuring tool to make reliable amplitude measurements. The tool incorporates techniques such as phase-match filtering and backazimuth calculation in order to reduce the noise contamination of fundamental Rayleigh-wave amplitudes. With the tool, we made surface-wave spectral-amplitude measurements for Asia and surrounding regions in the frequency band between 12 and 22 seconds. Using the amplitude measurements, we conducted tomographic inversions and developed 2D surface-wave attenuation-coefficient models from 12 to 22 seconds for the region.

We calibrated Russell (2006) surface-wave magnitude  $M_s$  using the 2D group-velocity model for Asia (Levshin *et al.*, 2003). Russell (2006)  $M_s$  calculated with Asia-specific parameters reduces the station-magnitude variance. The average magnitude is more consistent with the Rezapour and Pearce (1998)  $M_s$  used by IDC. We plan to conduct further calibration study of Russell (2006)  $M_s$  using the attenuation models that we developed.

## **ACKNOWLEDGEMENTS**

Seismograms used in this study are from the Incorporated Research Institutions for Seismology, Data Management Center. Some of the figures in this paper were plotted using the Generic Mapping Tool (Wessel & Smith, 1995)

## **REFERENCES**

Barmin, M. P., M. H. Ritzwoller, and A. L. Levshin (2001). A fast and reliable method for surface wave tomography, *Pure Appl. Geophys.*, Vol. 158, pp. 1351 - 1375.

- Bonner, J. L., D. R. Russel, D. G. Harkrider, D. T. Reiter, and R. B. Herrmann (2006). Development of a time-domain, variable-period surface wave magnitude measurement procedure for application at regional and teleseismic distances, *Bull. Seism. Soc. Am.* Vol. 96, pp. 678–696.
- Dziewonski, A., Chou, T.-A. & Woodhouse, J. H. (1981). Determination of earthquake source parameters from waveform data for studies of global and regional seismicity, *J. Geophys. Res.*, Vol. 86, pp. 2825-2852.
- Levshin, A. L. and M. H. Ritzwoller (2003). Discrimination, Detection, Depth, Location, and Wave Propagation Studies Using Intermediate Period Surface Waves in the Middle East, Central Asia, and the Far East, Technical Report DTRA-TR-01-28, Defense Threat Reduction Agency, 120 pp.
- Levshin, A. L., J. L. Stevens, M. H. Ritzwoller, D. A. Adams, and G. E. Baker (2003). Improvement of Detection and Discrimination Using Short Period (7s-15s) Surface Waves in W. China, N. India, Pakistan and Environs, Final Report, submitted to Defense Threat Reduction Agency, 49 pp.
- Levshin, A. L. (1985). Effects of lateral inhomogeneities on surface wave amplitude measurements., *Ann. Geophys.*, Vol. 3, No 4, pp. 511-518.
- Levshin, A. L., T. B. Yanovskaya, A. V. Lander, B. G. Bukchin, M. P. Barmin, L. I. Ratnikova, and E. N. Its (1989). *Seismic Surface Waves in Laterally Inhomogeneous Earth.* (Ed. V.I. Keilis-Borok), Kluwer Publ. House.
- Marshall, P. D. and P. W. Basham (1972). Discrimination between earthquakes and underground explosions employing an improved  $M_s$  scale, *Geophys. J. R. astr. Soc.* Vol. 28, pp. 431–458.
- Rezapour, M. and R. G. Pearce (1998). Bias in surface-wave magnitude  $M_s$  due to inadequate distance corrections, *Bull. Seism. Soc. Am.*, Vol. 88, pp. 43-61.
- Ritzwoller, M. H. and A. L. Levshin (1998). Eurasian surface wave tomography: Group velocities, *J. Geophys. Res.* Vol. 103, pp. 4839-4878.
- Russell, D. R. (2006). Development of a time-domain, variable-period surface wave magnitude measurement procedure for application at regional and teleseismic distances, Part I: Theory, *Bull. Seism. Soc. Am.* Vol. 96, pp. 665–677.
- Shapiro, N. M. and M. H. Ritzwoller (2002). Monte-Carlo inversion for a global shear-velocity model of the crust and upper mantle, *Geophys. J. Int.*, Vol. 151, pp. 88-105.
- Stevens, J. L., D. A. Adams, and G. E. Baker (2001). Improved surface wave detection and measurement using phase-matched filtering with a global one-degree dispersion model, in *Proceedings of the 23rd Seismic Research Review: Worldwide Monitoring of Nuclear Explosions*, LA-UR-01-4454, Vol. 1, 420-430.
- Vaněk, J., A. Zatopek, V. Karnik, N. V. Kondorskaya, Y. V. Riznichenko, E. F. Savarensky, S. L. Solov'ev, and N. V. Shebalin (1962). Standardization of magnitude scales, *Bull. Acad. Sci. USSR, Geophys. Ser.*, No. 2, pp. 108-111 (in English).
- von Seggern, D. H. (1977). Amplitude-distance relation for 20 second Rayleigh waves, *Bull. Seism. Soc. Am.*, Vol. 67, pp. 405-411.
- Wessel, P. A. and W. H. Smith (1995). New version of the generic mapping tools released, *EOS, Trans. Amer. Geophys. Un.* Vol. 76, Suppl., 329.
- Woodhouse, J. H. (1974). Surface waves in a laterally varying layered structure, *Geophys. J. Roy. Astr. Soc.*, Vol. 37, pp. 461-490.
- Yang, X., S. R. Taylor, and H. J. Patton (2004). The 20-s Rayleigh wave attenuation tomography for Central and Southeastern Asia, *J. Geophys. Res.*, Vol. 108, B12304, doi:10.1029/2004JB003193.